4.1 Introduction

Synthesis of metal nanoparticles stable against aggregation/agglomeration requires the use of stabilizers to provide steric or electrostatic stabilization [Zinsou and Fernandez (2010)]. The protecting/capping or stabilizing agents also strongly affects the size and shape of the nanoparticles. On the other hand, they also have electronic effects that can affect the catalytic properties of nanoparticles [Vilé *et al*. (2014)]. A few reports are available on catalytic effect of utilizing different stabilizers [Prieto *et al*. (2014), Santhanalakshmi and Parimala (2012)]. One such example is AuNPs stabilized by thiolated polyethylene glycol (S-PEG) as catalyst in 4-nitrophenol reduction. It was observed that there is a direct relationship between the chain length and packing density of S-PEG on AuNPs with catalytic activity. This high surface coverage of low molecular weight S-PEG inhibits the catalytic activity of AuNPs. By increasing molecular weight of S-PEG the surface coverage of NPs decreases and thereby increases the rate constant with decrease in induction time. Reports are available on catalytic effect of different stabilizers on Fischer-Tropsch Synthesis (FTS). Thus, trimethyl(tetradecyl)ammonium bromide (TTAB), polyvinylpyrrolidone (PVP), and sodium 3-mercapto-1-propanesulfonate (SMPS) were used as stabilizers for Ru/carbon nanofiber (CNF) catalysts. It was observed that the activity of these modified catalysts, having almost similar size in FTS, follow the order: Ru > Ru-TTAB > Ru-PVP >> Ru-SMPS. These results were correlated with the strength of stabilizer bond with Ru [Quek *et al*. (2013)]. Further, it was also reported that the ratio between metal ion salt to polymeric stabilizer also affects the reduction of metal ions and thereby the size of particles. Recently, Delgado *et al.* (2016) reported the effect of six different stabilizers on synthesis and catalytic property of cobalt nanoparticles (CoNPs) in

FTS reaction. Effect of stabilizers (starch, PVP, and PVA) is also reported on aerobic oxidation of 1,2-propanediol by hydrotalcite-supported platinum nanoparticles.

A variety of stabilizers are used for the synthesis of AgNPs. These have characteristic properties that make them fit for different applications in optical, electronic, chemical, biological, and medical fields [Lee *et al.* (2008a), Lee *et al.* (2008b), Ghosh and Pal (2007), Zeng *et al.* (2007), Tan *et al.* (2006), Pissuwan *et al.* (2006), Panigrahi *et al.* (2004)]. While there are many techniques for obtaining these nanoparticles, for environmentally friendly synthesis protocols, many researchers have turned toward natural substances such as vitamins, sugars, plant extracts, biodegradable polymers, and microorganisms as reducing and capping agents. Plant based materials seem to be the best candidates and they are suitable for large-scale 'biosynthesis' of nanoparticles [Song *et al.* (2009)]. The key or active agent in some of these synthesis are believed to be polyphenols. For instance, in tea, wine and winery waste, red grape pomace etc. [Georgiev *et al.* (2014), Dwyer *et al.* (2014)]. Similarly, curcumin, the main polyphenol in turmeric has recently been used as a stabilizing and reducing agent in synthesis of Au and Ag nanoparticles [Sindhu *et al.* (2014), Bettini *et al.* (2014), Sreelakshmi *et al.* (2013)]. Curcumin possess long conjugation and multiple functional groups in its molecular structure. These are responsible for its reducing and capping ability [Sindhu *et al.* (2014), Bettini *et al.* (2014), Sreelakshmi *et al.* (2013)].

As discussed in previous chapter, the visible range LSPR absorbance of AgNPs is size dependent. Further curcumin also absorbs visible light. There are very few reports on use of curcumin as a sensitizer [Lim *et al.* (2017), Moussawi and Patra (2016)]. Curcumin derived dyes have been used as sensitizer in dye sensitized solar cells [Ganesh *et al.* (2010)]. They have also been applied as sensitizers for detecting cancerous cell [Xiao-ai *et*

al. (2017), Wang *et al.* (2017)]. Recently it was reported that curcumin possesses better photochemical and photoelectrochemical activities than RuL_3/TiO_2 which is frequently employed as a visible light sensitizer. Here curcumin acts as photo sensitizer and enhances the photocatalytic activity delaying the recombination of energetic charge carriers.

There does not seem to have reports related to curcumin stabilization of noble metal nanoparticles and their effects on catalytic properties. Keeping this in perspective, this chapter presents a detailed study on the catalytic activity of curcumin stabilized silver nanoparticles (c-AgNPs). The catalytic efficiency of c-AgNPs was tested by using them as catalysts in reactions i) *p*-nitrophenol (Nip) to *p*-aminophenol (AP) with sodium borohydride ($NaBH_4$), ii) Nip reduction by glycerol (Gly), iii) Oxidative degradation of methyl orange (MO). Investigations are carried out from two perspectives. One, for elucidating the effect of increased curcumin stabilization on the normal catalytic properties of c-AgNPs. The effect of temperature on kinetics of Nip reduction and MO oxidation is also studied. Next, to understand the effect of visible light irradiation on photocatalytic properties of c-AgNPs. Here also two AgNPs samples with different amounts of curcumin stabilization are considered. This helps in understanding the extent of photosensitizing properties of curcumin on the overall photocatalytic properties of these c-AgNPs.

This chapter first presents the preparation of c-AgNPs by an ultrasound assisted green synthesis protocol. Ultrasound assisted or sonochemical reduction route for this synthesis was explored to overcome the disadvantage of longer reaction times [Patil *et al.* (2008)] generally associated with green synthesis protocols. In sonochemical techniques acoustic cavitation due to high intensity ultrasonic irradiation of water leads to formation of highly reactive $H^\bullet$ and $OH^\bullet$ radicals. Sonochemically generated $H^\bullet$ radicals or secondary radical species from organic additives in the reaction mixture are considered to act as

reductant in such metal nanoparticle synthesis [Bang and Suslick (2010)]. c-AgNPs with two different size distributions were prepared by taking different amounts of curcumin in the synthesis. Next, these two c-AgNPs samples were applied as catalysts in the reduction of Nip to AP by $NaBH_4$ and Gly. The efficacy of these catalysts for Fenton like oxidative degradation of MO was also investigated. Finally, the effect of carrying out these reactions under visible light irradiation was also studied. These c-AgNPs are found to exhibit excellent catalytic and photocatalytic activities for the reactions investigated.

4.2 Experimental

4.2.1 Synthesis of curcumin stabilized AgNPs (c-AgNPs)

Materials used for the synthesis of c-AgNPs were $AgNO_3$ (Merck), Curcumin (Sigma Aldrich) and NaOH (Merck). All reagents used were of analytical reagent grade and used without further purification. Curcumin solutions of 0.01 M and 0.001 M concentration were prepared by dissolving suitable amount of curcumin in 2 mL of 10 mM aqueous NaOH solution and then the volume was made up to 10 mL by water. Next, 5 mL each of these freshly prepared curcumin solutions were added to 0.05 mmol of $AgNO_3$ taken in 40 mL water and subjected to ultrasonication for 5 min (with 25 sec 'on' and 10 sec 'off' cycles). On completion of this treatment the reaction mixture turned from yellowish red to greenish yellow which indicated the formation of c-AgNPs. Hereafter, the c-AgNPs samples prepared are denoted as A1 when the precursor silver salt to curcumin ratio was taken as 1 : 1. The same procedure was repeated to obtain A2 c-AgNPs, with silver salt precursor to curcumin ratio 1 : 0.1.

4.2.2 Catalytic reduction and oxidation

4.2.2.1 Catalytic Nip reduction with NaBH₄

The experimental details for the Nip reduction with $NaBH_4$ in presence of A1 and A2 c-AgNPs is identical to the protocol described in sub-section 3.2.2.1 of Chapter-3.

4.2.2.2 Catalytic Nip reduction with glycerol

The particulars of experiments for the Nip reduction with Gly as reductant in presence of A1 and A2 c-AgNPs as catalyst is identical to the protocol described in sub-section 3.2.2.2 of Chapter-3.

4.2.2.3 Catalytic oxidation of MO dye

The experimental details for the oxidative MO degradation with H_2O_2 in presence of A1 and A2 c-AgNPs is identical to the protocol described in sub-section 3.2.2.3 of Chapter-3.

4.2.3 Visible light enhancement of catalytic reduction and oxidation activites

Photocatalytic activity is measured by placing the reaction mixtures in photocatalytic chamber as described in Chapter-2. The temperature of the photocatalytic chamber was measured to be 306 K.

4.2.3.1 Photocatalytic enhancement of Nip reduction with glycerol

The reaction mixture with the catalyst was prepared as given in section 3.2.2.2, this is then irradiated by visible light from cool white LED source (approximately 940 watts/m^2) in the photocatalytic chamber at 306 K. The absorption spectrum of the reaction mixture was recorded after every 10-minute time interval.

4.2.3.2 Photocatalytic oxidation of methyl orange dye

The reaction mixture with the catalyst was prepared as given in section 3.2.2.3. The reaction mixture was kept in the photocatalytic chamber at 306 K and then irradiated by visible light from cool white LED source (approximately 940 watts/m^2). The kinetics and photocatalytic activities were measured for all c-AgNPs catalysts samples in this manner.

4.3 Results and Discussion

4.3.1 Characterization of c-AgNPs

Figure 4.1 shows the UV-Visible absorbance spectrum of the as-prepared (diluted) A1 and A2 c-AgNPs sols. For both A1 and A2 c-AgNPs sols, the maximum UV-visible absorbance was found to be ~ 408 nm which is in agreement with the well-known LSPR absorbance of aqueous dispersion of silver nanoparticles [Vasileva *et al*. (2011)].
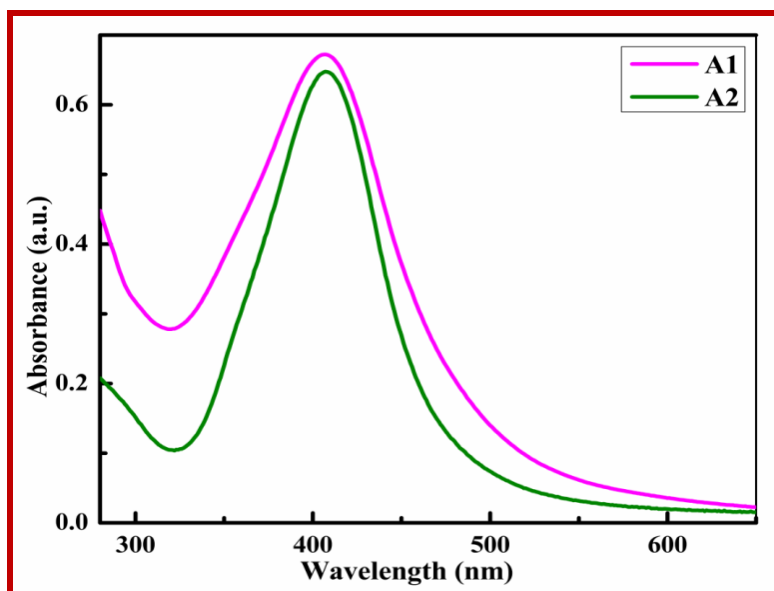
Figure 4.1 The UV-visible absorption spectra of aqueous dispersions of samples A1 (10 times diluted) and A2 (as prepared) c-AgNPs sols.

The X-ray diffraction pattern of the powdered A1 and A2 c-AgNPs samples are shown in Figure 4.2. As per the data reported for FCC silver in JCPDS-ICDD (card no. 87-

0720), five peaks were observed at 38.18, 44.40, 64.66, 77.07 and 81.25 which correspond to {111}, {200}, {220}, {311} and {222} reflections respectively.
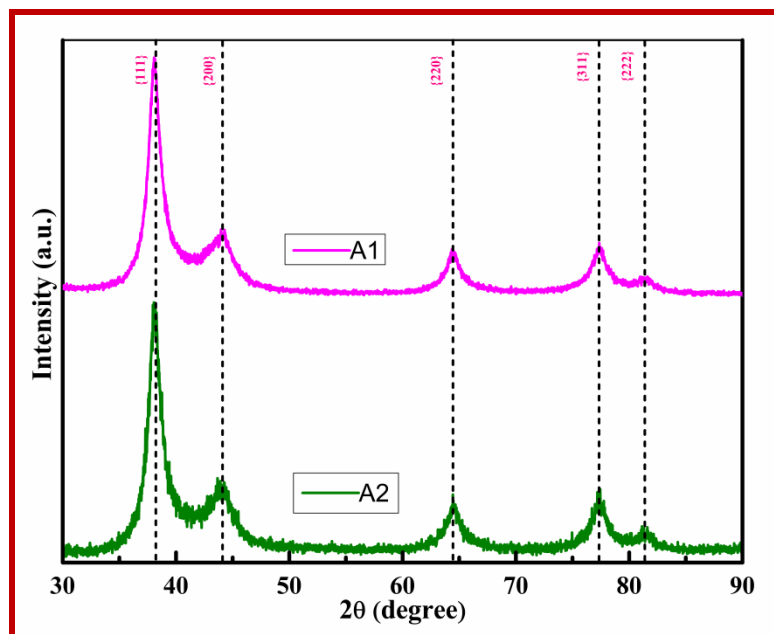
Figure 4.2 X-ray powder diffraction patterns of A1 and A2 c-AgNPs samples.

TEM micrographs and their respective particle size distributions of A1 and A2 c-AgNPs samples are shown in Figure 4.3. In A1 c-AgNPs sample particles are found to be uniformly spherical in shape with an average size of ~ 17 nm, it is indicated by the size distribution histogram (Figure 4.3 (b)). On the other hand, A2 c-AgNPs sample have narrower size distribution as well as finer average particle size of ~ 12 nm, size distribution histogram was shown in Figure 4.3 (d). The size of nanoparticles was calculated from the TEM micrographs. The average particle size of c-AgNPs samples were calculated by measuring approximately 300 nanoparticles.
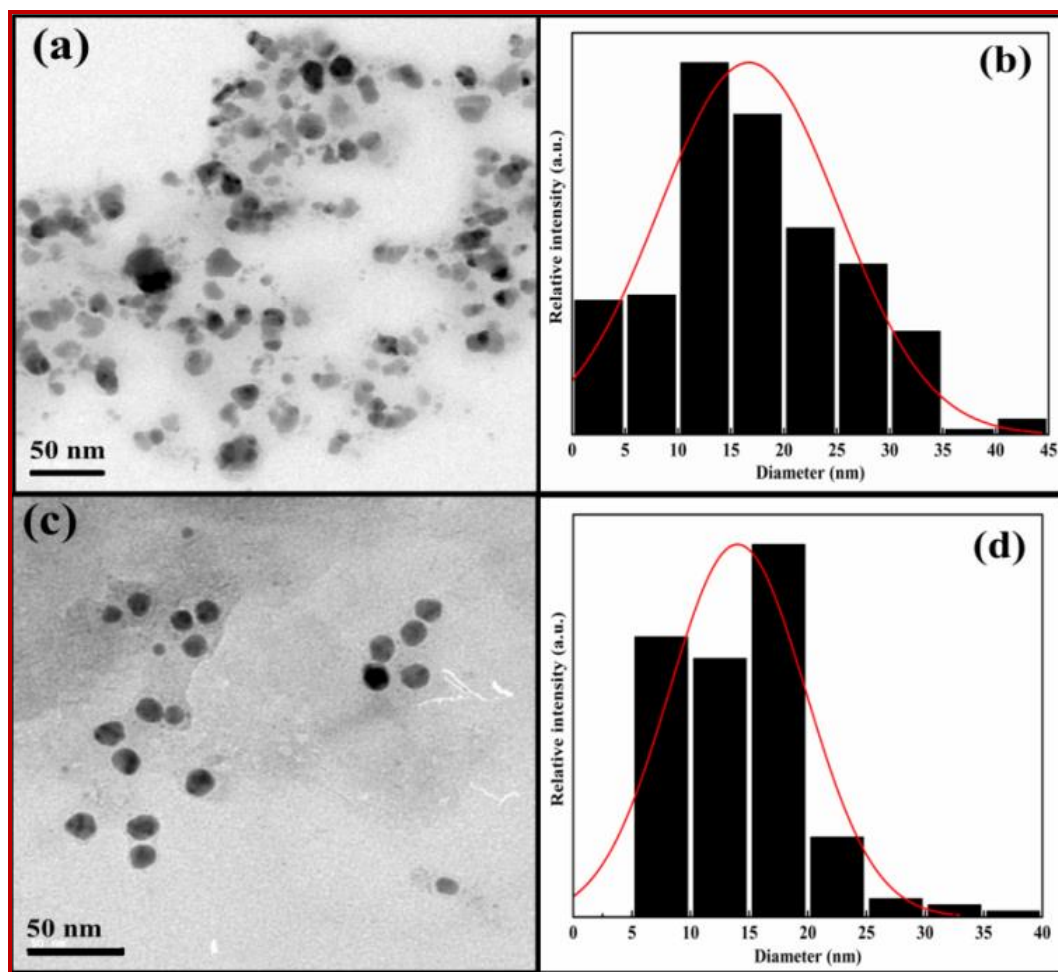
Figure 4.3 TEM image of samples A1 and A2 of c-AgNPs (a, c), and the corresponding size distributions (b, d), respectively.

For analyzing the interactions between c-AgNPs and functional groups associated with curcumin, the FTIR spectra of both pure curcumin and solid powder c-AgNPs (A2) sample (Figures 4.4 (a) and 4.4 (b)) were recorded in the range of 4000–400 cm^{-1} in the diffuse reflectance mode, operating at resolution of 1 cm^{-1} using Perkin Elmer Spectrum 100 FT-IR spectrometer. To obtain a good signal to noise ratio, 16 scans of c-AgNPs were taken using KBr pellets. As can be seen from a comparison of the FTIR spectra of curcumin and c-AgNPs, the bands at 2922 cm^{-1}, 1462 cm^{-1}, 1030 cm^{-1} and 959 cm^{-1} that appear in c-AgNPs are due to vibrations of aliphatic C–H stretches and mixed vibrations of

CH_3, aromatic CCC and CCH bonds present in curcumin. This confirms that curcumin acts as a capping agent [Sindhu *et al*. (2014)].
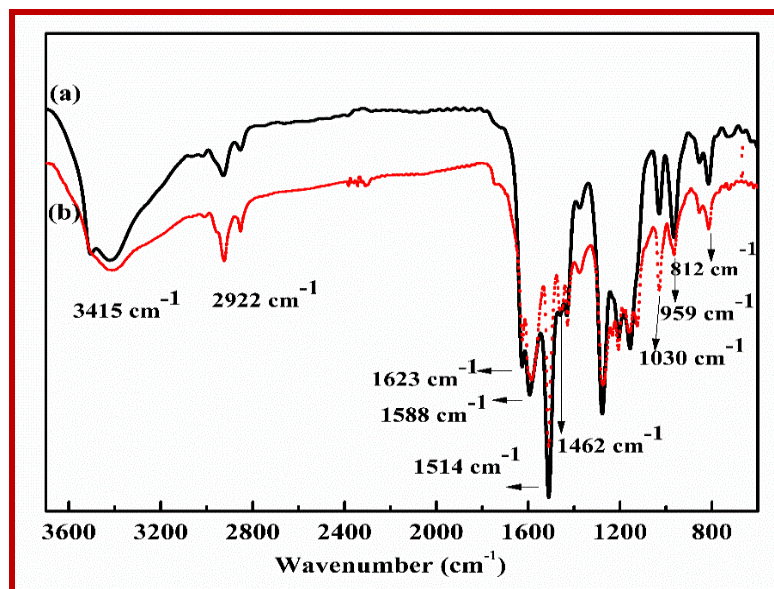

Figure 4.4 FT-IR spectra of (a) pure curcumin and (b) curcumin stabilized AgNPs (sample A2 c-AgNPs).

4.3.2 Catalytic study

4. 3.2.1 c-AgNPs catalyzed Nip reduction with NaBH₄ and glycerol

Figure 4.5 (a) displays Nip reduction with $NaBH_4$ as reducing agent in presence of A2 c-AgNPs. The intensity of the absorption peak at ~ 401 nm decreased with progress of time. Simultaneously, a smaller absorbance peak at ~ 300 nm emerged and gradually increased due to the formation of the reaction product *p*-aminophenol (AP). Also, the spectrum showed two isosbestic points at ~ 280 and ~ 312 nm which indicates that Nip was converted to AP without any side reaction.

Furthermore, it was observed that on completion of the reaction, the absorption peak originally at ~ 401 nm undergoes slight blue shift and its intensity does not go to zero (Figure 4.5 (a)).
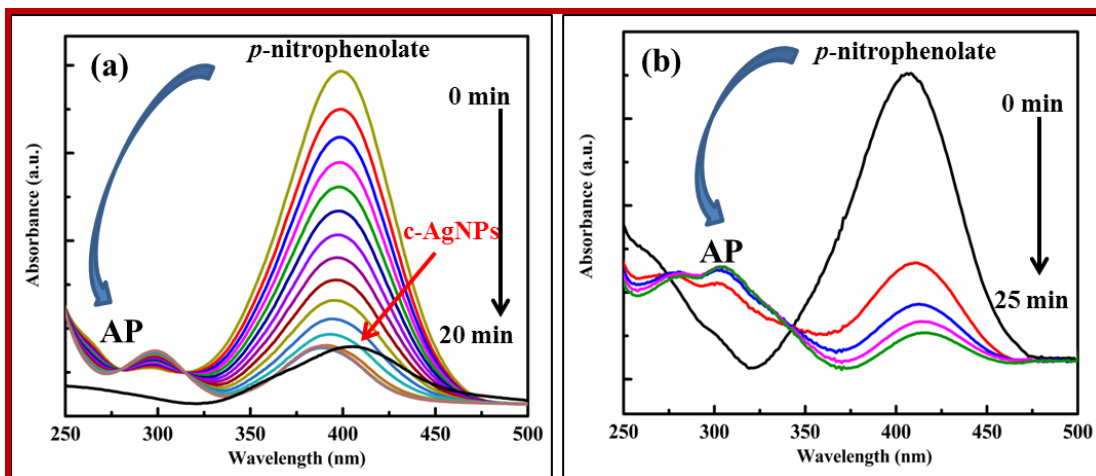
Figure 4.5 Variation of absorbance maximum of *p*-nitrophenolate (~ 401 nm) with NaBH$_4$ (a) and absorbance maximum of *p*-nitrophenolate (~ 406 nm) with Gly (b) as reductant in presence of c-AgNPs catalyst.

The remaining absorbance at this slightly blue shifted maximum is due to the LSPR of the c-AgNPs since the intensity of this absorbance was the same as that of the aqueous dispersion of c-AgNPs used for catalysis (shown in Figure 4.5 (a)). As is well-known, the blue shift of the LSPR absorbance is due to the adsorption of *p*-nitrophenolate ions on the surface of the silver nanoparticles [Pradhan *et al.* (2001), Henglein (1989)].

Figure 4.5 (b) displays the UV-visible spectra for Nip reduction in presence of glycerol as reductant with A2 c-AgNPs as the catalyst. The absorbance maximum at ~ 406 nm (due to formation of *p*-nitrophenolate ion) decreased with time, while the absorbance peak at ~ 306 nm was found to increase with time. The absorbance maximum at ~ 306 nm indicates the formation of AP (Figure 4.5 (b)). However, in contrast to Nip reduction with NaBH$_4$, in this case the isosbestic points are not clear. Therefore, further characterization was carried out to confirm the formation of AP. This was done in two parts. First, the azo-dye test was done to qualitatively affirm the formation of the aromatic amine functional group as per the procedure given in reference [Vogel (1978)]. The formation of orange

colored azo dye showed the presence of the amine functional group. The final confirmation of AP formation was by analysis of the ^{1}HNMR spectrum of the product (Figure 4.6). ^{1}HNMR was measured in DMSO. The NMR peaks observed are δ 8.35 (s, 2 H), 7.27 – 5.02 (m, 4 H), 4.38 (s, 2 H). These correspond to the three types of H present in AP.
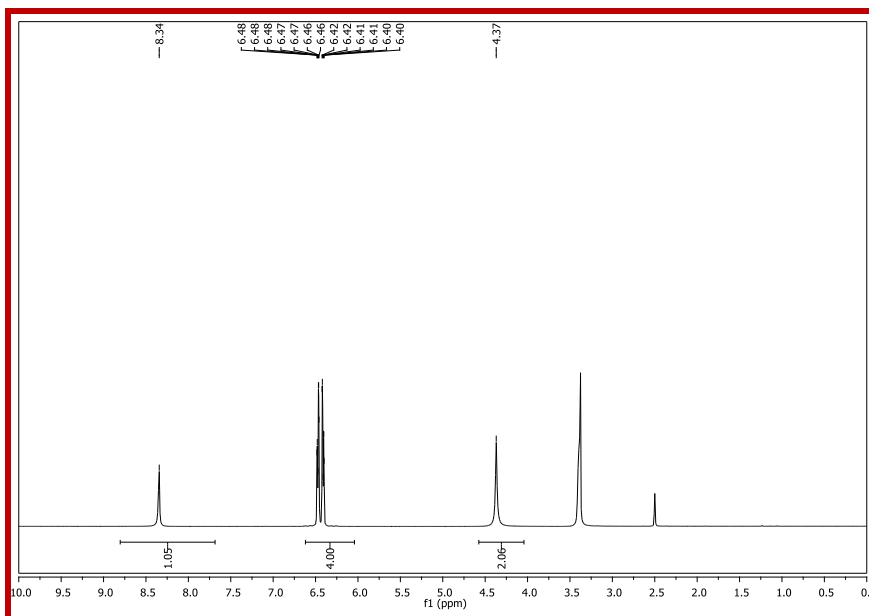

Figure 4.6 NMR spectrum of product of Nip reduction with glycerol in presence of A1 c-AgNPs.

Reduction kinetics

As the amount of the reducing agent NaBH$_4$ is in much larger excess (almost 40 times) than Nip concentration taken, therefore the concentration of the reductant remains almost constant during the reaction. The order of the reaction was found by the procedure adopted in section 3.3.2.2 of Chapter-3. That is, the slope of the linear fit of plot between $\ln\left(-\frac{\partial A}{\partial t}\right)$ versus $\ln(A)$ [from Eqn. 3.3], considering only the data points after the elapse of the t_{ind}, gives the order of the reaction [Alla *et al.* (2016), Gu *et al.* (2014)]. The value of n is found to be 1 when NaBH$_4$ is the reductant. This suggests the reduction

follows pseudo first order kinetics. Corresponding to this, plots between $\ln(A/A_0)$ and time (when $NaBH_4$ is the reducing agent) for A1 and A2 c-AgNPs catalyzed reactions are given in Figure 4.7 (a)). On monitoring the absorbance of p-nitrophenolate ion, it is observed that initially it did not change for some interval of time (Figure 4.7 (a)). The time during which no reduction took place is known as induction time (t_{ind}) and it was observed that the reaction started only after the elapse of t_{ind} [Aditya et al. (2015)]. The possible reason for this is due to adsorption of oxygen in aqueous medium on to the surface of c-AgNPs [Signori et al. (2010)].
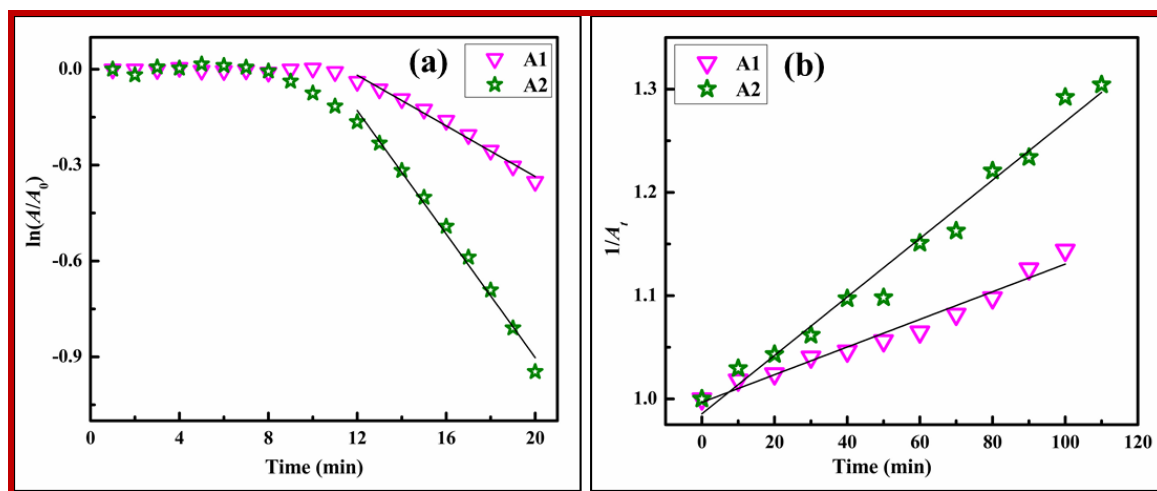

Figure 4.7 Variation of $\ln(A/A_0)$ [absorbance (A) measured at ~ 401 nm] Vs time with $NaBH_4$ reductant **7(a)**. Variation of $1/A_t$ [absorbance (A) measured at ~ 406 nm] Vs time with Gly as reductant in presence of both c-AgNPs catalyst **7(b)**. The R^2 value of all the fittings is ~0.98.

The data after the elapse of the initial induction time shows good linear fits in accordance with first order kinetics. The slope of this linear fit gives the k_{app} value. As mentioned earlier, Nip reduction by $NaBH_4$ is a model reaction. Accordingly, there are a number of reports on different catalysts that have been employed to study the kinetics of this reaction. Since majority of them follow pseudo first order kinetics, therefore, these

observations are in agreement with previously published data in literature [Deka *et al.* (2014), Yang *et al.* (2014)].

On the other hand, when Gly was the reducing agent, the value of slope of the plot between $\ln\left(-\frac{\partial A}{\partial t}\right)$ versus $\ln(A)$ is 2 [using Eqn. 3.3]. This is the same as obtained previously in Chapter-3 for Nip reduction with glycerol. Plots of $1/A_t$ versus time (for A1 and A2 c-AgNPs catalyzed Nip reductions) have good linear fits (Figure 4.7 (b)). The k_{app} values were determined from the slopes of the linear fit of $(1/A_t)$ against time. There was no induction time when Gly was the reducing agent. This may be due to lower relative solubility of oxygen [Signori *et al.* (2010)] in aqueous solution of glycerol as compared to pure water.

The activation energies involved, were determined by the linear form of Arrhenius equation [Eqn. 3.4]. Figure 4.8 (a) shows ln k_{app} versus 1/T plots for A1 and A2 when NaBH$_4$ was the reducing agent.
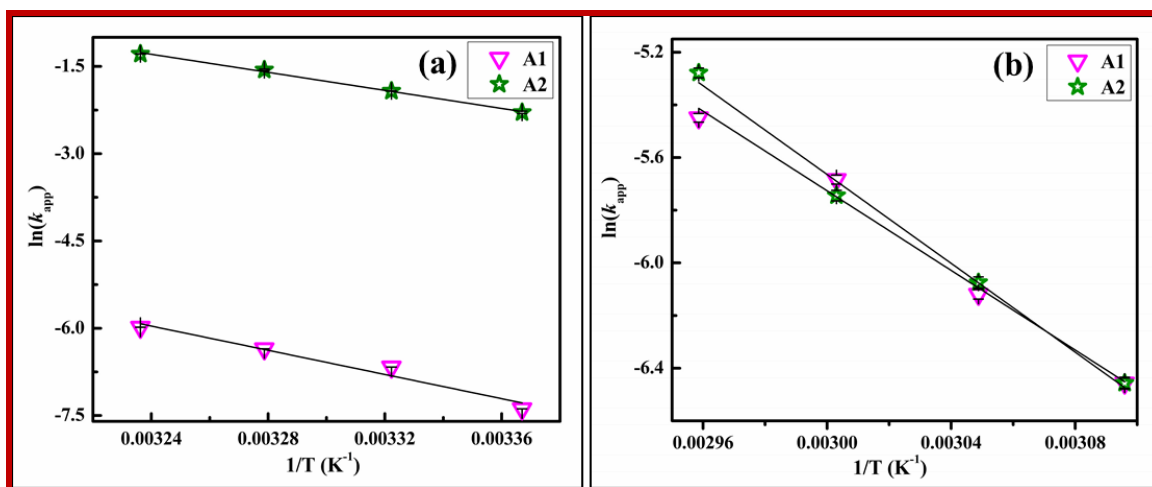
Figure 4.8 Arrhenius plot for Nip reduction reaction catalyzed by A1 and A2 c-AgNPs samples with reducing agents NaBH$_4$ (a) and Gly (b). Error bars are very small in most of the cases. The R^2 value of all the fittings is ~ 0.98.

The slope ($-E_a/R$) of the linear fit gives the corresponding activation energy (E_a). Activation energy plots between $\ln(k_{app})$ and $1/T$ for Gly reduced reactions are displayed in Figure 4.8 (b). Table 4.1 gives the average catalyst particle sizes, the k_{app} values and activation energies. The order of the reaction when $NaBH_4$ was the reductant was pseudo first order, while it was second order with Gly as the reductant. Therefore, the k_{app} values for different catalysts are comparable only for the same reductant. The first important observation is that the average nanoparticle size of A1 is greater than that of A2. This means that A2 has more surface area or more access due to more active sites. The activation energy for A1 is also greater than A2. Therefore, both surface area and activation energy values support the higher catalytic activity observed for A2. Similarly for Gly reduced reactions, the k_{app} value for A2 c-AgNPs catalyst is again higher. However, the E_a value for A2 is greater than that found for A1. This means that the number of active sites is more in A2 due to the lower particle size and high surface area in A2 sample. Moreover, this effect dominates the catalytic activity.

Table 4.1 Average particle size, apparent reaction rate constants and activation energy for Nip reduction with $NaBH_4$ and Gly reducing agent in presence of both A1 and A2 c-AgNPs catalyst.

Catalyst	Particle size	Apparent reaction rate constant (k_{app})		Activation energy (E_a) (kJ/mol)	
	d (nm)	$NaBH_4$ (min^{-1})	Gly (mol^{-1} lit min^{-1})	$NaBH_4$	Gly
A1	~ 17	0.0392	0.00134	~ 86.3	~ 63.1
A2	~ 12	0.0966	0.00283	~ 65.4	~ 70.2

As discussed earlier turnover frequency (TOF) is a more appropriate quantity to define the catalytic activity of the nanomaterials used as catalysts. Therefore, TOF are calculated for both catalysts using Eqn. 3.5. TOF values for A1 and A2 c-AgNPs catalysts for Nip reduction in presence of $NaBH_4$ as the reducing agent are tabulated in Table 4.2 and are also compared with the values available in literature for Nip reduction with $NaBH_4$. The Table shows that among the various catalysts, for which such data is available in literature (Table 4.2), the present c-AgNPs catalyst has the best TOF values.

Earlier Chang *et al.* (2012) and Baruah *et al.* (2013) reported the use of Ag nanoparticles of comparable size as catalysts for Nip reduction by $NaBH_4$. The TOF values calculated from their publications are much lower than those found for c-AgNPs in the present investigation [Baruah *et al.* (2013), Chang *et al.* (2012)].

Table 4.2 Comparison of turnover frequencies (TOF) for *p*-nitrophenol reduction by $NaBH_4$.

Sr. No.	Catalyst	Turnover Frequency (TOF) (min^{-1})	Reference
1	CuNPs	~ 0.0122	[Deka *et al.* (2014)]
2	Au/Graphene hydrogel	~ 68.4	[Li *et al.* (2012)]
3	Au on PMMA	~ 0.5	[Kuroda *et al.* (2009)]
4	Au NCs	~ 0.3	[Rashid *et al.* (2006)]
5	Au on Carbon nanotubes	~ 0.1	[Fattah and Wixtrom (2014)]
6	AgNPs	~ 40.2	[Chang *et al.* (2012)]
7	AgNPs/PANINF	~ 202	[Chang *et al.* (2012)]
8	AgNP-PG-5K	~ 320	[Baruah *et al.* (2013)]
9	Au-MgO	~ 0.4	[Layek *et al.* (2012)]
10	c-AgNPs (A1)	~ 1081	This work
11	c-AgNPs (A2)	~ 1600	This work

* The TOF values mentioned in table are calculated by the Eqn. 3.5 utilizing the data available in literature

A possible reason could be that curcumin on being attached to the metal acts in some synergistic way (with respect to the catalyst being an electron conduit for Nip reduction) to increase number of catalytic active sites per unit surface area of the catalyst [Priyadarsini (2014)]. The extended conjugated electronic structure of curcumin means that the π electron cloud is delocalized over the entire molecule. This feature of curcumin may be related to the enhancement of catalytic activity of c-AgNPs.

The TOF values of Gly reduced Nip reactions also follow the same trend, that is, the TOF value of A2 is greater than that of A1 (Table 4.3). The measurements were done at 306 K and there are no reports in literature on catalyzed Gly reduction of Nip at this temperature. Therefore, this will be discussed in comparison to the photocatalytic activity, in the following sub-section.

4.3.2.2 Photocatalytic study

The thermal Nip reduction with Gly follows second order kinetics which is similar to previous observation when anisotropic AgNPs were used as catalyst. In contrast to this, the photocatalytic Nip reduction with glycerol follows zero order kinetics (Figure 4.9). This implies that the mechanism followed in the visible light photocatalytic Gly reduction of Nip is different from that followed in absence of light. Since the photocatalytic reaction follows zero order, therefore, the k_{app} values are obtained from the slope of the linear fit of A/A_0 versus time plot.
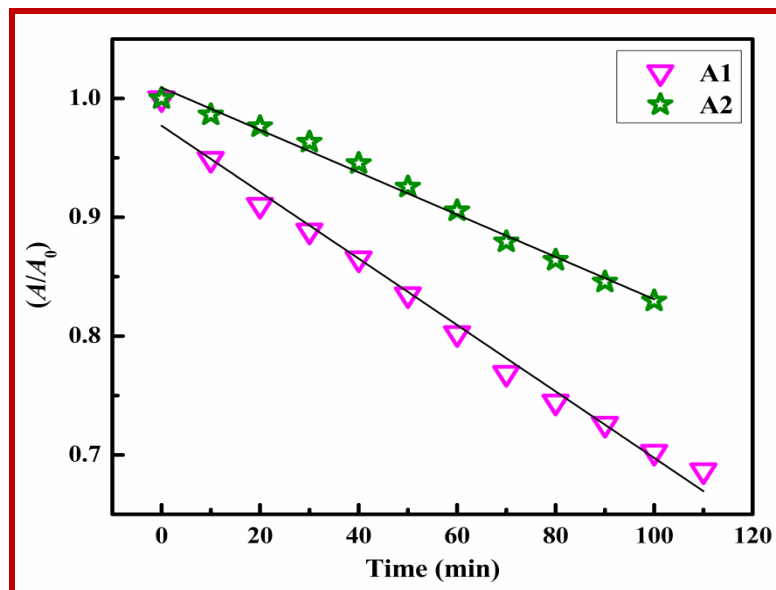
Figure 4.9 Variation of A/A_0 [absorbance (A) measured at ~ 406 nm] versus time in photocatalytic Nip reduction with Gly. The R^2 value of all the fittings is ~ 0.98.

The k_{app} values of photocatalytic Nip reduction with glycerol are tabulated in column 2 of Table 4.3. This shows that A1 c-AgNPs has higher k_{app} compared to A2. The PTOF values show the same trend. In fact, the PTOF of A1 is more than double the value obtained for A2. For the sake of comparison, the TOF values of c-AgNPs catalyzed Gly reduction of Nip without light (but at the same temperature, 306 K) are given in the same Table 4.3. As mentioned earlier, in this case A2 shows higher TOF than A1. Moreover, the PTOF value for A1 is more than five times the TOF value A1. The photocatalytic enhancement in case of A2 is lesser. These observations and that the order of the photocatalytic reaction is different, suggest that the basic mechanism of Nip reduction with Gly is not same when it is carried out under visible light irradiation.

Table 4.3 The photocatalytic apparent reaction rate constant, photocatalytic turnover frequency (PTOF) and TOF for Nip reduction with Gly as reducing agent at 306 K.

Catalyst	Apparent reaction rate (k_{app}) (mol lit^{-1}min^{-1})	Turn over frequency (TOF) (min^{-1})	
		TOF	PTOF
A1	0.0028	~ 3.9	~ 22.0
A2	0.0018	~ 5.7	~ 12.0

To understand the possible mechanism involved, it is important to note that the curcumin used in the preparation of A1 c-AgNPs was ten times the amount for synthesis of sample A2. Clearly, the amount of curcumin functionalized on the surface of A1 nanoparticles must be higher than A2. Conventionally, it has been shown that increase in amount of stabilizer on the surface of the nanocatalyst inhibits the approach of the substrate molecule [Quek *et al.* (2013)]. However, in the present investigation the results are exactly the reverse. That is, higher curcumin (stabilizer) presence on the surface of the AgNPs increases the photocatalytic activity. Therefore, it can be surmised that the curcumin stabilizing the AgNPs surfaces take part in the photocatalytic reaction as a photosensitizer. A plasmonic mechanism similar to that given in Chapter-3 may also be acting in conjunction with this.

### 4.3.2.3 Methyl orange oxidation: thermal and photocatalytic

Figure 4.10 shows the UV-visible spectrum of MO degradation when the reaction is carried out in presence of A2 c-AgNPs. All three peaks present initially in the UV-visible spectrum of MO in acidic medium undergo degradation together with progress of time. Moreover, there is no sign of any new absorption in these regions.
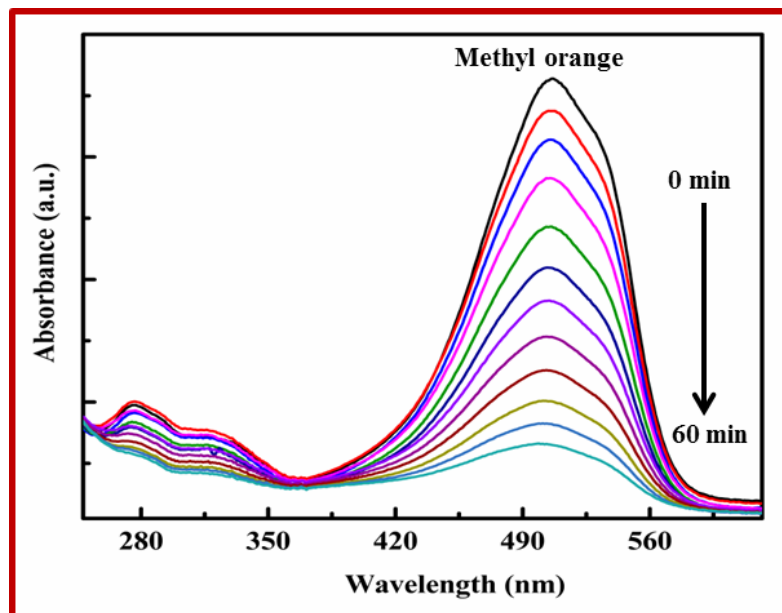
Figure 4.10 Variation of absorbance maximum of MO (~ 506 nm) with H_2O_2 oxidizing agent in presence of catalyst A2 c-AgNPs catalyst.

The slope of the linear fit of plot between $\ln(-\frac{\partial A}{\partial t})$ versus $\ln(A)$ [Eqn. 3.3] gives the order of MO degradation. The order, thus calculated, are 2 and 0 for thermally and photocatalytically catalyzed MO degradation respectively. Consequently, the respective k_{app} values are found from the slopes of the linear fits for the plots between $1/A_t$ versus time for thermal and A/A_0 versus time photocatalytic MO degradations (Figure 4.11).

Linearized Arrhenius plots between $\ln(k_{app})$ and 1/T for the thermally catalyzed reactions are displayed in Figure 4.12. The activation energy Ea is calculated from the slope of the linear fit of this graph. Table 4.4 presents the k_{app}, TOF and PTOF values of both thermal and photocatalytic MO degradations. The E_a values for A1 and A2 c-AgNPs are also given in column 4 of this Table. Again, it is important to note that the orders of the thermal and photocatalyzed reactions are different. Hence, their k_{app} values cannot be compared with each other.
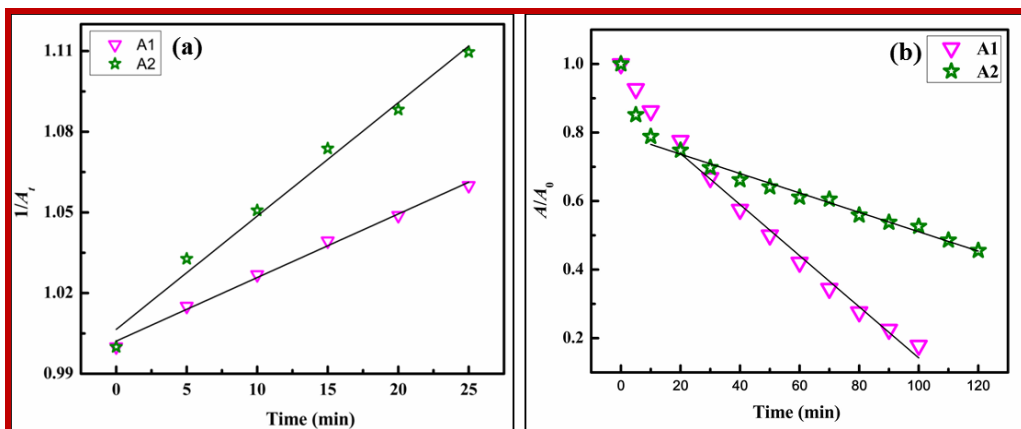
Figure 4.11 Variation of $1/A_t$ [absorbance (A) measured at ~ 506 nm] versus time for thermal (a) and photocatalytic (b) MO degradation in presence of A1 and A2 c-AgNPs catalyst. The R^2 value of all the fittings is ~ 0.97.
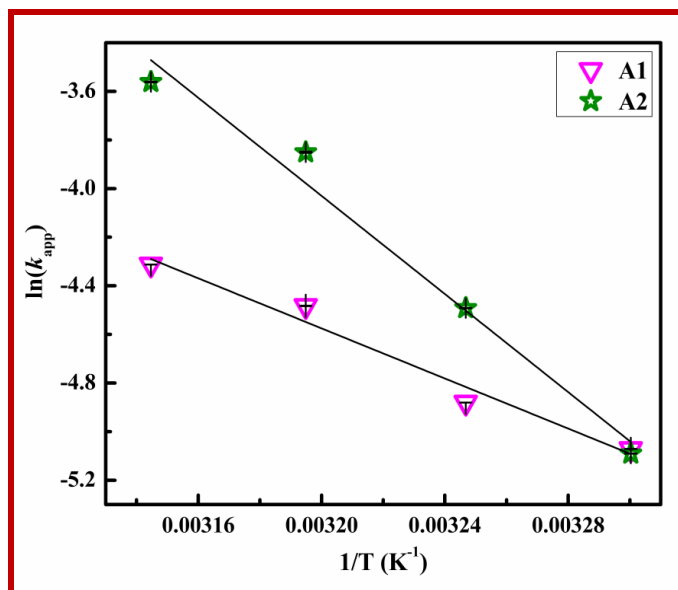
Figure 4.12 Arrhenius plot for MO degradation catalyzed by A1and A2 c-AgNPs samples. Error bars are very small in most cases. The R^2 value of all the fittings is ~ 0.98.

Thus, comparison is only made between different catalysts when rests of the reaction conditions are the same. The k_{app} value for A2 c-AgNPs is higher than A1 in thermal oxidative degradation of MO. Surprisingly, the activation energy (E_a) of A1 is half

of the value calculated for A2. Thus, a higher thermal catalytic activity of A2 is primarily due to larger number of active sites available on it. As mentioned earlier, this is consequence of its smaller average nanoparticle size and thereby higher surface area.

Table 4.4 Apparent reaction rate constant, activation energy and turnover frequency (TOF) for thermal and photocatalytic MO degradation at 306 K in presence of both c-AgNPs catalyst

Catalyst	Apparent reaction rate (k_{app}) (mol lit^{-1} min^{-1})		Activation energy (E_a) (kJ/mol)	Turn over frequency (TOF) (min^{-1})	
	Thermal	**Photo**		**TOF**	**PTOF**
A1	0.00236	0.00745	~ 42.2	~ 0.9	~ 5.1
A2	0.00421	0.00268	~ 84.3	~ 1.4	~ 2.8

The PTOF values from A1 and A2 show a trend which is exactly the reverse of the results obtained from the catalytic reaction in absence of light. This trend is similar to that obtained in case of photocatalytic Nip reduction by Gly. Since A1 has higher amount of curcumin functionalized on it, therefore, it indicates that this stabilizer acts like a photosensitizer in this case as well. To know the active species involved in this process, p-benzoquinone (PBQ), potassium iodide (KI) and isopropyl alcohol (iPA) were used as scavengers to capture superoxide radical (O_2^-), holes, and hydroxyl radicals ($^{\cdot}OH$) respectively. Figure 4.13 shows the results of this experiment.
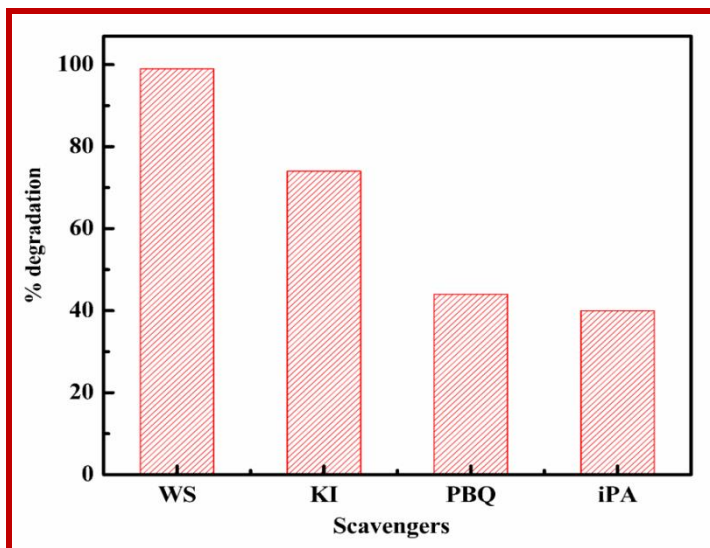
Figure 4.13 Percentage photocatalytic MO degradation without scavenger (WS) and in presence of KI, PBQ and iPA scavengers.

Degradation efficiency gets affected both by addition of iPA and PBQ, which shows that the main active species for this reaction are both hydroxyl ($^{\cdot}$OH) and superoxide radicals ($O_2^{\cdot-}$). The Fermi level of Ag lies between the HOMO and LUMO of curcumin. It appears that photosensitization of curcumin is facilitated by some surface Ag atoms getting oxidized. That is, electrons generated from this oxidation are used to quench the holes in the HOMO of curcumin. The excited electrons may be participating in the formation of superoxide radicals ($O_2^{\cdot-}$).

On the other hand, direct oxidation of surface Ag atoms of the nanoparticle may also take place. That is, visible light LSPR absorbance by AgNPs leads to formation of energetic charge carriers. These electrons are then directly transferred from higher energy levels in the metal to the adsorbate resulting in formation of hydroxyl radicals. In this case, the visible light plasmonic excitation possibly facilitates step (2) of the reaction mechanism

given in sub-section 3.3.2.3. The oxidized surface Ag atoms are reduced back in step (5) resulting in regeneration of AgNPs.

4.4 Conclusions

Two different size distributions of fine curcumin stabilized silver nanoparticles have been synthesized using a sonochemical protocol. Nanoparticle size distribution became narrower and average sizes finer on increasing the ratio of precursor silver salt to curcumin. The catalytic activities of these nanoparticles in absence and presence of visible light were investigated on the *p*-nitrophenol reduction and MO oxidation. Silver nanoparticles with finer size distribution (sample A2) demonstrated significantly better catalytic activity. For c-AgNPs catalyzed reduction of Nip by NaBH$_4$, the activation energy of A1 was higher than that of A2. However, when the reducing agent was Gly, the trend gets reversed. That is, the E_a value of A2 is higher. Same trend was obtained for oxidative degradation of MO. However, in all these cases the higher surface area and thereby higher number catalytic active sites in A2 dominates the proceedings. Thus, in all thermally catalyzed cases, the catalytic activity of A2 is more.

The conventional reaction with NaBH$_4$ as the reducing agent follows pseudo first order kinetics. Whereas, this reaction with glycerol as hydrogen source follows second order kinetics with respect to Nip. The photocatalytic enhancement in A1 c-AgNPs is more than five times its thermal reaction due to both plasmonic effect of c-AgNPs and presence of excess curcumin which acts as sensitizer. MO oxidation also follows second order kinetics in thermal and zero order in photocatalytic reaction. Photocatalytic MO degradation also shows enhancement in PTOF compared to thermal TOF values in presence of both A1 and A2 c-AgNPs catalyst.